
Article:
Chen, L., Chen, C., Sun, Y. et al. (8 more authors) (2020) Luminescent metallacycle-cored liquid crystals induced by metal coordination. Angewandte Chemie International Edition, 59 (25). pp. 10143-10150. ISSN 1433-7851

https://doi.org/10.1002/anie.201915055

RESEARCH ARTICLE

Luminescent Metallacycle-Cored Liquid Crystals Induced by Metal-Coordination

Long Chen, Changlong Chen, Yue Sun, Shuai Lu, Haohui Huo, Tianyi Tan, Anquan Li, Xiaopeng Li, Goran Ungar, Feng Liu * and Mingming Zhang *

1. Pre-accepted version. Published in *Angew. Chem. Int. Ed.* 2020 http://dx.doi.org/10.1002/anie.201915055

[*] L. Chen, C. Chen, Y. Sun, H. Huo, T. Tan, Prof. Dr. G. Ungar, Prof. Dr. F. Liu, Prof. Dr. M. Zhang
State Key Laboratory for Mechanical Behavior of Materials, Shaanxi International Research Center for Soft Matter, School of Materials Science and Engineering,
Xi'an Jiaotong University, Xi'an 710049 (P. R. China)
E-mail: mingming.zhang@xjtu.edu.cn, feng.liu@xjtu.edu.cn

Dr. Y. Sun
Hubei Key Laboratory of Catalysis and Materials Science, College of Chemistry and Material Sciences,
South-Central University for Nationalities, Wuhan 430074 (P. R. China)

S. Lu, Prof. Dr. X. Li
Department of Chemistry, University of South Florida, Tampa, FL 33620 (USA)

S. Lu
College of Chemistry, Zhengzhou University, Zhengzhou, Henan 450001 (P. R. China)

A. Li
School of Chemistry, Sun Yat-Sen University, Guangzhou, 510275 (P. R. China)

Supporting information for this article is given via a link at the end of the document.

Abstract: Direct construction of supramolecular coordination complexes with both luminescent and mesogenic properties is a contemporary challenge. Herein we report two rhomboidal metallacycles based on metal-coordination-driven self-assembly. Because metal-coordination interactions restrict the rotation of phenyl groups on tetraphenylethene units, these metallacycles were emissive both in solution and in solid state, and their aggregation-induced emission properties were well retained. Moreover, the rhomboidal metallacyclic structures offer a platform for intermolecular packing beneficial for the formation of liquid crystalline phases. Therefore, although neither of building blocks shows mesogenic properties, both thermotropic and lyotropic (in DMF) mesophases were observed in one of the metallacycles. indicating that mesophases could be induced by metal-coordination interactions. This study not only reveals the mechanism for the formation of cavity-cored liquid crystals, but also provides a convenient approach to preparing supramolecular luminescent liquid crystals, which will serve as good candidates for chemo sensors and liquid crystal displays.

Introduction

Luminescent Liquid crystals (LCs) have received much attention during the last two decades due to their broad applications in optoelectronics.[1] A general approach to construct luminescent LCs is to introduce mesogenic units onto a rigid fluorescent core to combine luminescent and mesogenic properties together.[2] In this regard, the efficiency of the luminophores is a key problem because the intermolecular interactions at high concentrations or in the solid states will normally give a pathway for non-radiative decay to quench the emission, leading to weakened luminescence for the devices. In 2001, Tang et. al. reported a new type of fluorophores which is nearly non-emissive in dilute solution while emits strongly at high concentrations or in the solid state, opening a new area termed as "aggregation induced emission (AIE)" materials.[3] When the AIE fluorophores are incorporated in luminescent LCs,[4] the aggregation of the molecules in the devices will promote the emission of the fluorophores, benefiting for the construction of luminescent LCs with high contrast ratio and deep color saturation.

Metal-coordination-driven self-assembly has proved to be an efficient approach to prepare supramolecular coordination complexes (SCCs),[5,6] including metallacycles and metallacages with specific geometries due to their high directionality and moderate bond strength. The integration of luminescence into SCCs provides a series of emissive metallacycles and metallacages[7] with interesting optical properties. Especially, emissive SCCs derived from AIE fluorophores[7] take the advantages of the metal-coordination bonds to restrict the intramolecular motions (rotations or vibrations) of AIE molecules, thus benefiting the resulted SCCs good emission properties both in solution and in the solid state, which are of vital importance for their practical applications. The Stang group pioneered this study by using tetraphenylethene (TPE, a typical AIE molecule) derivatives to prepare a series of emissive SCCs[7] and explored their applications as chemo-sensors,[8] light-emitting materials,[9] contrast agents for bioimaging[10], light-harvesting[11] and so on. Yang, Li and co-workers reported the preparation of emissive

rosette-shaped SCCs using multitopic terpyridine-functionalized TPE as ligands, in which pure white-light emission could be generated from one of the SCCs.[12]

Although much progress has been made on the emissive SCCs,[7-12] SCCs with both luminescent and mesogenic properties have been rarely reported yet.[13] The formation of liquid crystal phases by SCCs calls for dense molecular packing, which normally quenches the emission. Moreover, branched chains are needed to fill the empty spaces induced by the packing of SCCs due to their empty cavities. The stabilities of the SCCs are also a key problem especially for thermotropic liquid crystals. Herein, we prepared a dipyridyl TPE derivative decorated with branched alkyl chains which doesn't show any mesophases either in solution or in the molten conditions. However, when it was used as an organic donor to assemble with a tri(ethylene glycol)-functionalized 60° diplatinum(II) compound, the formed rhomboidal metallacycle exhibits both thermotropic and lyotropic (in DMF) mesophases as evidenced by polarized optical microscopy (POM) and synchrotron radiation-based small/wide angle X-ray scattering (SAXS/WAXS). The inside metallacyclic structures stack on top of one another to form columns, while the outer alkyl and tri(ethylene glycol) chains fulfil the empty space to induce the formation of mesophases. Considering the inherent luminescent properties of the SCC derived from TPE units,[3d] luminescent metallacycle-cored liquid crystals were successfully constructed. This study offers an example to demonstrate how the formation of metallacyclic structures influences the intermolecular packing and thus organizes them into ordered phases, providing a new type of SCCs as luminescent LCs which may be used in chemical sensing and LC displays.

Results and Discussion

Synthesis and characterization of rhomboids

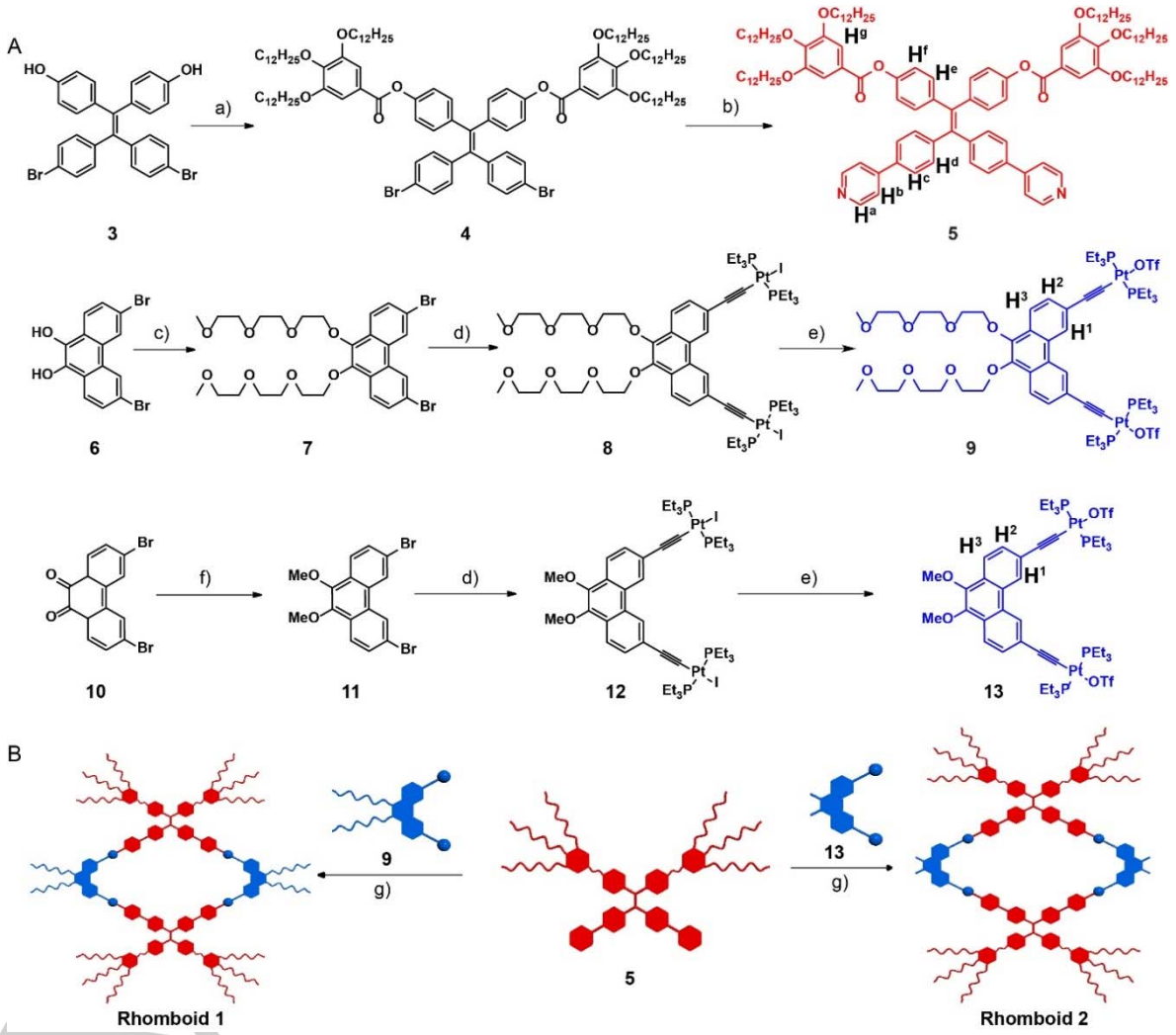

Scheme 1. (A) Synthetic routes and chemical structures of the compounds used in this study. (B) Cartoon representations for the formation of metallacyclic rhomboids **1** and **2** via the metal-coordination-driven self-assembly. Reaction conditions: a) 3,4,5-tris(dodecyloxy)benzoic acid, 1-ethyl-3-(3-dimethylaminopropyl)carbodiimide (EDC), 4-dimethylaminopyridine (DMAP), CH_2Cl_2, room temperature; b) pyridine-4-boronic acid, K_2CO_3, $Pd(PPh_3)_4$, tetra-*n*-butylammonium iodide (TBAI), toluene/ethanol/water (4:1:1), reflux; c) triethylene glycol monomethyl ether, K_2CO_3, CH_3CN, reflux; d) (i) trimethylsilyl acetylene,

$Pd(PPh_3)_4$, CuI, toluene, reflux; (ii) KF, MeOH/THF(1:1), room temperature; (iii) $Pt(PEt_3)_2I_2$, CuI, toluene, room temperature; e) AgOTf, CH_2Cl_2, room temperature; f) (i) $Na_2S_2O_4$, tetra-*n*-butylammonium bromide (TBAB), THF/H_2O (1:1); room temperature; (ii) NaOH, Me_2SO_4, room temperature; g) dichloromethane, room temperature.

The synthetic procedures of metallacyclic rhomboids **1** and **2** were depicted in Scheme **1.** The esterification of a previously reported compound **3**[10] with tris(dodecyloxy)benzoic acid gave intermediate **4**, which was further transferred into a 120° dipyridyl TPE derivative **5** *via* a classical Suzuki coupling reaction with pyridine-4-boronic acid. Diplatinum (II) acceptors **9** and **13** were prepared in reasonable yields from commercially available compound 3,6-dibromophenanthrene-9,10-dione (**10**). Rhomboids **1** and **2** were then prepared in nearly quantitative yield by stirring dipyridyl compounds **5** with corresponding diplatinum(II) acceptor **9** or **13** in dichloromethane at room temperature overnight.

Rhomboids **1** and **2** were carefully characterized by $^{31}P\{^1H\}$, ^1H and diffusion-ordered (DOSY) NMR spectroscopy, and electrospray ionization time-of-flight mass spectrometry (ESI-TOF-MS). In the $^{31}P\{^1H\}$ NMR spectra (Figure 1, A-D), singlet peaks with obvious upfield chemical shifts (21.85 ppm for **9**; 21.81 ppm for **13**; 15.88 ppm for rhomboid **1**; 15.90 ppm for rhomboid **2**) were observed for rhomboids **1** and **2** compared with their precursors **9** and **13**, which is a characteristic property of the formation of metal-coordination bonds. In the ^1H NMR spectra (Figure 1, E-I), the *α*-pyridyl protons H^a split into two set of peaks and the *α*-pyridyl protons H^a, *β*-pyridyl protons H^b, aromatic protons H^c and H^d shifted downfield, which is consistent with previously reported results[10] and indicates the formation of rhomboidal metallacycles **1** and **2**. DOSY spectra (Figures S37 and S41) indicate the formation of single assemblies by these two metallacycles because all of the proton signals exhibit the same diffusion coefficient (*D*) with $D = 1.12 \times 10^{-8}$ $cm^2 \cdot s^{-1}$ for rhomboid **1** and $D = 1.29 \times 10^{-8}$ $cm^2 \cdot s^{-1}$ for rhomboid **2.**

ESI-TOF-MS gave evidence of the stoichiometry for the formation of rhomboidal metallacycles. Peaks at m/z = 1622.6801, 2213.0188, 2538.6570 and 3393.6602 were found for rhomboid **1** (Figure 1J), corresponding to the charge states [**1** – **4**OTf]$^{4+}$, [**1** – **3**OTf]$^{3+}$, [**1** – **9** – 2OTf]$^{2+}$, [**1** – 2OTf]$^{2+}$, respectively. Similarly, peaks at m/z = 1489.5753, 2036.5194, 2407.0435 and 3129.4133 were observed for rhomboid **2** (Figure 1K), corresponding to [**2** – 4OTf]$^{4+}$, [**2** – 3OTf]$^{3+}$, [**2** – **13** – 2OTf]$^{2+}$, [**2** – 2OTf]$^{2+}$, respectively. All the peaks were isotopically well-resolved and consistent with their calculated theoretical distributions.

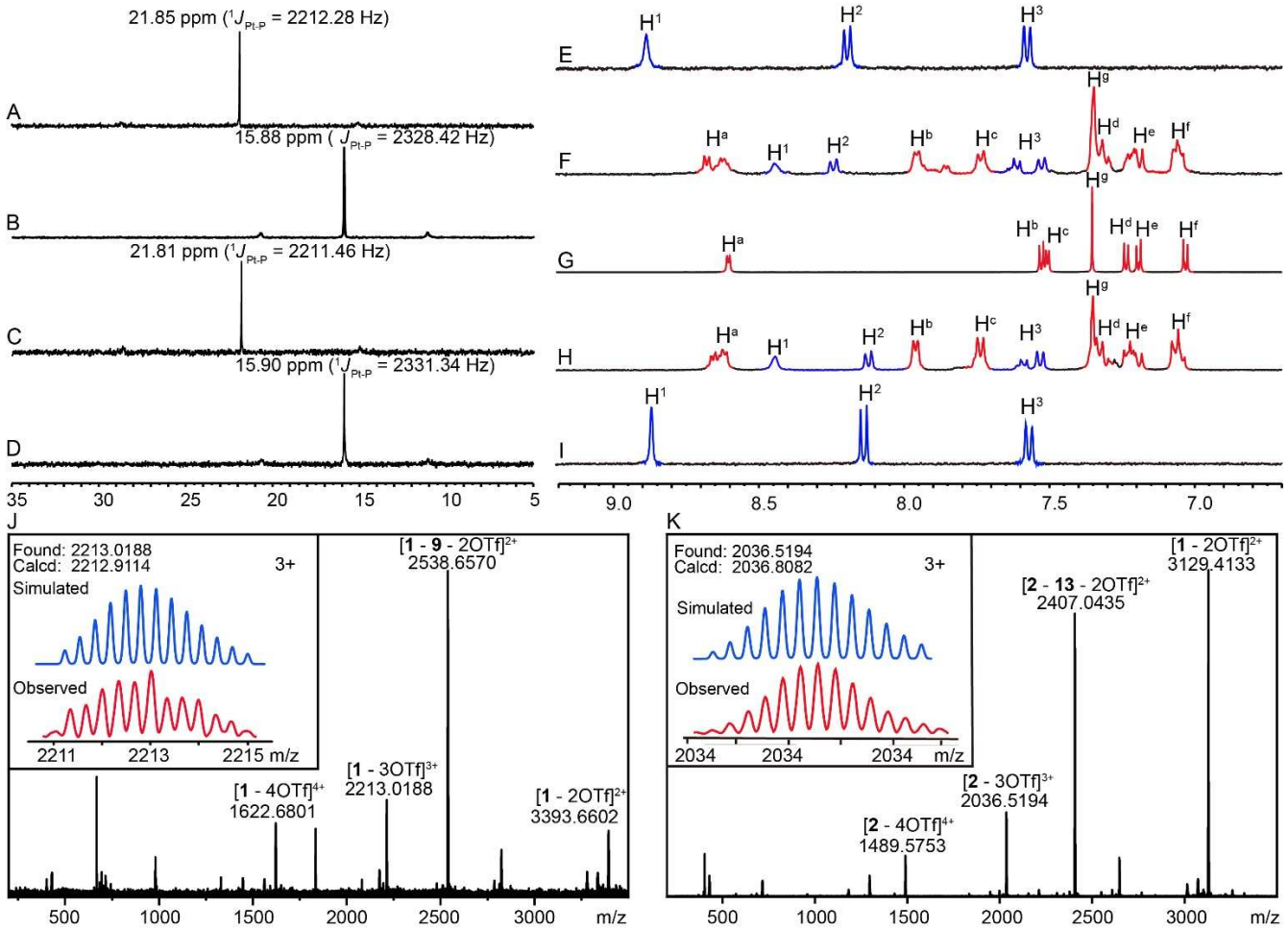

Figure 1. Partial (A-D) $^{31}P\{^1H\}$ and (E-I) ^1H NMR spectra (CD_2Cl_2, 295 K) of diplatinum(II) acceptor **9** (A and E), **13** (C and I), rhomboid **1** (B and F), rhomboid **2** (D and H) and dipyridyl ligand **5** (G). ESI-TOF-MS spectra of rhomboid **1** (J) and rhomboid **2** (K). Inset: Experimental (red) and calculated (blue) ESI-TOF-MS spectra of [M – 3OTf]$^{3+}$.

Photophysical properties.

After the chemical structures and compositions of rhomboids **1** and **2** were proved, the photophysical properties of the building blocks (**5**, **9** and **13**) and the complexes (**1** and **2**) in dichloromethane were then collected by UV/Vis absorption and fluorescence spectroscopy. It can be seen from the absorption spectra (Figure 2A) that diplatinum(II) acceptors **9** and **13** exhibit four similar absorption bands centered at 265 nm, 307 nm, 353 nm and 370 nm, with molar absorption coefficients (ε) of 5.81 × 10^4 $M^{-1}\cdot cm^{-1}$, 2.09 × 10^4 $M^{-1}\cdot cm^{-1}$, 1.91 × 10^4 $M^{-1}\cdot cm^{-1}$, 1.68 × 10^4 $M^{-1}\cdot cm^{-1}$ for **9**, 6.31 × 10^4 $M^{-1}\cdot cm^{-1}$, 2.42 × 10^4 $M^{-1}\cdot cm^{-1}$, 2.36 × 10^4 $M^{-1}\cdot cm^{-1}$, 2.02 × 10^4 $M^{-1}\cdot cm^{-1}$ for **13**, respectively. Dipyridyl ligand **5** displays an absorption band centered at 276 nm with ε of 7.27×10^5 $M^{-1}\cdot cm^{-1}$. The absorption spectra of rhomboids **1** and **2** are also similar, showing four absorption bands centered at 275 nm, 307 nm, 350 nm and 368 nm with ε of 2.56 × 10^5 $M^{-1}\cdot cm^{-1}$, 1.61 × 10^5 $M^{-1}\cdot cm^{-1}$, 1.37 × 10^5 $M^{-1}\cdot cm^{-1}$, 1.31 × 10^5 $M^{-1}\cdot cm^{-1}$ for rhomboid **1**, 2.30 × 10^5 $M^{-1}\cdot cm^{-1}$, 1.43 × 10^5 $M^{-1}\cdot cm^{-1}$, 1.24 × 10^5 $M^{-1}\cdot cm^{-1}$, 1.19 × 10^5 $M^{-1}\cdot cm^{-1}$ for rhomboid **2**, respectively.

The fluorescence spectra are shown in Figure 2B. Diplatinum(II) acceptors **9** and **13** are nearly non-emissive in dichloromethane. Dipyridyl ligand **5** shows a broad emission band centered at 568 nm, almost 100 nm red shift compared with TPE,[7b] indicating that the branched alkyl chains strongly influence the emission. After metal-coordination, rhomboids **1** and **2** exhibit strong emission bands centered at 544 nm and 553 nm, respectively.

The emission intensities and quantum yields (Φ_F) of rhomboids **1** and **2** in dichloromethane and dichloromethane/hexane mixtures were recorded to investigate their AIE characteristics (Figure 2, C-E). Rhomboids **1** and **2** were completely soluble in dichloromethane and moderate emission were observed upon excitation at 365 nm. As the gradual addition of poor solvents (hexane), the emission intensity gradually increased (Figure S42). No significant enhancement in emission was seen when the hexane volume content is lower than 60%. However, dramatical increment of emission was observed and reached maximum when the hexane volume fraction (V/V%) is 90%, indicating that rhomboids **1** and **2** are typical AIE fluorophores. At high hexane fractions, the free rotation of the phenyl groups of the TPE units are strictly inhibited due to molecular aggregation (Figure S43), which will reduce the non-radiative decay and provide enhanced emission for the system. The measurements of quantum yields (Figure 2E) in different hexane fractions further support the AIE characteristics of rhomboid **1** and **2**. Their Φ_F values in pure dichloromethane were measured to be 1.12% and 0.92%, respectively. When the hexane fraction increased into 50%, these values increased to 1.73% and 1.26%, respectively. At the hexane fraction of 90%, their Φ_F values increased to 8.37% and 6.38%, respectively. In the film state, the Φ_F values are 12.6% and 7.6% for rhomboids **1** and **2**, respectively (Figure 2F). All these results supported the AIE characteristics of rhomboids **1** and **2**.

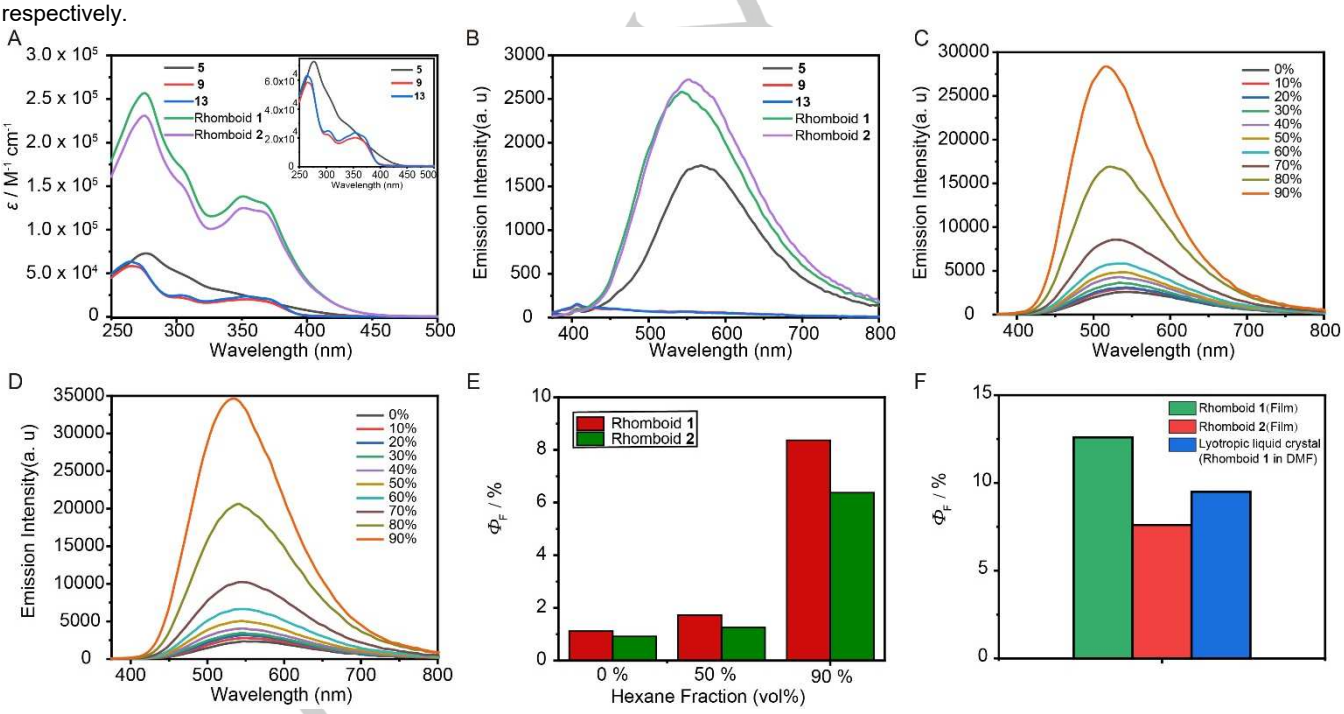

Figure 2. (A) UV-vis absorption and (B) fluorescence spectra of ligand **5**, diplatinum(II) acceptors **9** and **13** and rhomboids **1** and **2** in dichloromethane. (C, D) Fluorescence spectra of rhomboids **1** and **2** versus hexane fraction in dichloromethane/hexane mixtures. Quantum yields of rhomboids **1** and **2** versus hexane volume fraction in dichloromethane/hexane mixtures (E) and in the film and liquid crystal state (F). (λ_{ex} = 365 nm, c = 10.0 μM).

Self-assembly of rhomboids 1 and 2 in water.

The self-assembly behavior of rhomboids **1** and **2** in aqueous solution was further studied. Due to their poor solubility in water, they were first dissolved into tetrahydrofuran (THF) and then diluted with water (5.0 μM, 1% THF in water). The critical aggregation concentration (CAC) of amphiphilic rhomboid **1** was determined to be 1.23 × 10^{-6} M by plotting the optical transmittance of aqueous solutions of rhomboid **1** at 420 nm versus concentration (Figure S44). However, the CAC of

rhomboid **2** cannot be measured using the same method due to its hydrophobic nature. The size and shape of these nanoparticles were further studied by transmission electron microscopy (TEM), scanning electron microscopy (SEM) and dynamic light scattering (DLS) measurements. Dark grey, round-shaped particles with an average diameter of 86 nm were observed by TEM (Figure 3A) for amphiphilic rhomboid **1** at the concentration of 5.0 μM, consistent with the spherical micellar structures with an average diameter of 95 nm obtained by SEM (Figure 3B). However, irregular aggregates for rhomboid **2** with average diameter of 90 nm were observed at the concentration of 5.0 μM (Figure 3E and 3F), suggesting the hydrophobicity of rhomboid **2**. The DLS measurements gave hydrodynamic diameters (D_h) of ~114 nm for rhomboid **1** and ~110 nm for rhomboid **2** (Figure 3C and 3G), respectively, consistent with the TEM and SEM results. More importantly, due to the emission of the two rhomboidal metallacycles **1** and **2** (Figure S45), their assemblies could be also observed by confocal laser scanning microscopy (CLSM). Dispersed nanoparticles with bright blue emission were observed for rhomboid **1** (Figure 3D) while fluorescence from aggregates of nanoparticles were clearly observed for rhomboid **2** (Figure 3H), which agree well with the amphiphilic and hydrophobic nature of rhomboids **1** and **2**, respectively.

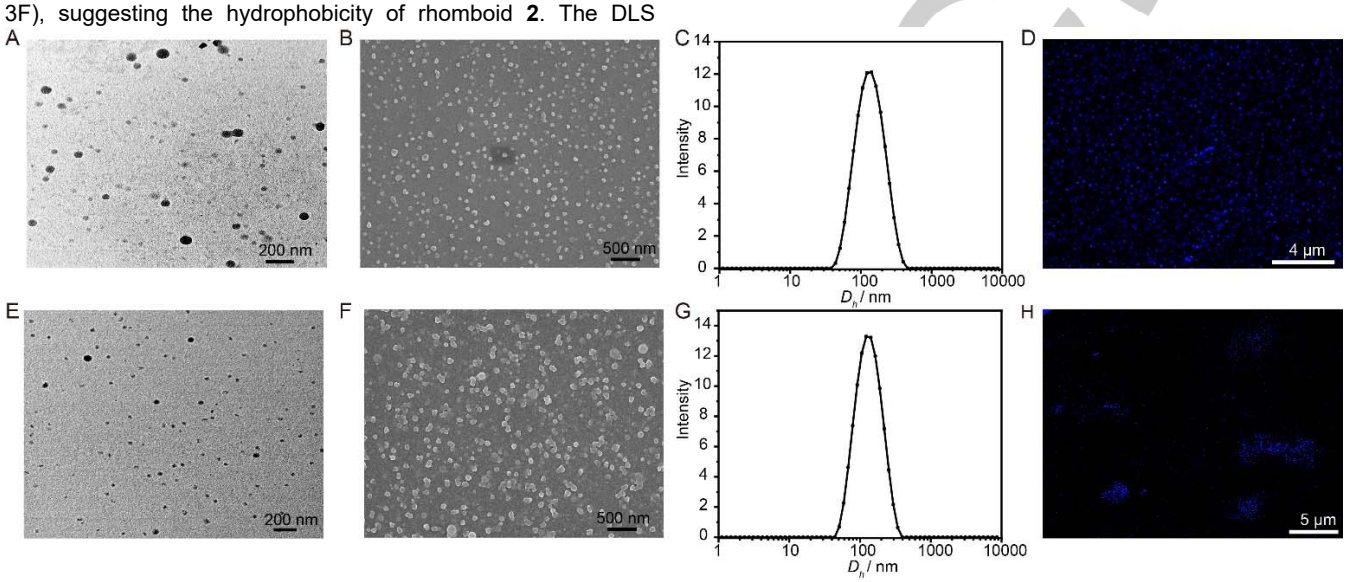

Figure 3. (A, E) TEM images, (B, F) SEM images, (C, G) DLS and (D, H) confocal laser fluorescence images of rhomboid **1** (A-D) and rhomboid **2** (E-H) (c = 5.0 μM).

Liquid-Crystalline Properties.

Ligand **5**, diplatinum (II) acceptors **9** or **13** do not show any liquid crystal (LC) phase either in solution or in the molten state. However, clear birefringence was observed with a polarizing microscope for rhomboid **1** (Figures 4A and S48) while no such phenomenon was found for rhomboid **2** in the liquid state, suggesting that rhomboid **1** can form thermotropic mesophases. WAXS diffractograms of rhomboid **1** over a wide temperature range show only one diffuse scattering peak (Figure S49B), which is typical for LC phases, indicating that the individual molecules do not have fixed positions. Rhomboid **1** is stable from 30 to 110 °C, as suggested by the temperature-dependent NMR experiments (Figures S52 and S53). The SAXS diffractograms obtained from the powder samples are shown in Figures 4B and S49A. The sharp Bragg peaks in SAXS are indexable on a 2D rectangular lattice with *c*2*mm* symmetry, the unit cell parameters being a = 11.80 nm and b = 6.50 nm (Table S1). The reconstructed electron density (ED) map further confirms the formation of the Col_{rec}/*c*2*mm* structure (Figure 4C). The method of selecting the correct phase combination is described in Section XXX of the Supporting Information. In the map, the metallacycles are surrounded by terminal alkyl and tri(ethylene glycol) groups of medium average ED (blue), having a low ED central pore (red). A hight ED rim (purple) surrounds the pore, coming from the Pt atoms. It is nearly circular in shape due to orientational averaging.

When polar solvent, such as DMF, was added into rhomboid **1**, birefringent texture were observed by polarizing microscopy at a concentration of 18.0 mM (Figure 4D), indicating that rhomboid **1** can also form a lyotropic LC phase (Φ_F = 9.5%). The powder scattering pattern shows six sharp reflections with a 1/d ratio of 1: $3^{1/2}$: 2: $7^{1/2}$: 3: $19^{1/2}$. This indicates a hexagonal lattice (*p*6*mm*) with a lattice parameter a_{hex} = 6.82 nm (Figure 4E and Table S2). In the wide-angle region, two diffuse peaks were observed at 4.7 Å and 3.9 Å (inset in Figure 4E), which are contributions from the peripheral alkyls/tri(ethylene glycol) chains and π-π stacking of the adjacent aromatic cores, respectively. The additional peak at 3.9Å, which was not observed in the thermotropic Col_{rec}/*c*2*mm* phase, proves that the addition of polar solvent can improve the π-π stacking of conjugated cores. As can be seen from the ED map (Figure 4F), in the lyotropic Col_{hex}/*p*6*mm* phase, Pt ED maxima are also surrounding the central cavity, but this time they are more localized in six spots responsible for the star-like appearance of the column centres in Figure 4F. The positions of the Pt atoms are indicated in Figures 4F and 4I. The ED maps thus support the existence of a pore in the centre of the column, as suggested by the molecular model in Figure 4I and SXXX. Such pore-forming structures have also been reported for a number of systems with stable LC structures. [14]

Notably, there is a broad SAXS peak marked with an asterisk alongside the sharp Bragg peak in both thermotropic and lyotropic LC phases formed by rhomboid **1** (Figure 4B and 4E).

Considering the presence of tri(ethylene glycol) chains in rhomboid **1,** potassium trifluoromethanesulfonate (KOTf) was added to test the origin of the peak, as potassium ions where expected to complex with ethylene glycol chains and thus increase the ED contrast. The molar ratio of rhomboid **1** and KOTf was 1:2. SAXS diffractograms of rhomboid **1** without and with KOTf are shown in Figure S50. The addition of KOTf is seen to strengthen the broad peak about 3 times more than the Bragg one, confirming that the diffuse peak originates in clusters of ethylene glycol chains. The reason that the peak is diffuse is in the domains of separated alkyl and tri(ethylene glycol) chains being distributed with local rather than long range order (Figure 5G). The local fluctuations give rise to the diffuse SAXS peak, as reported before for a different system.[15]

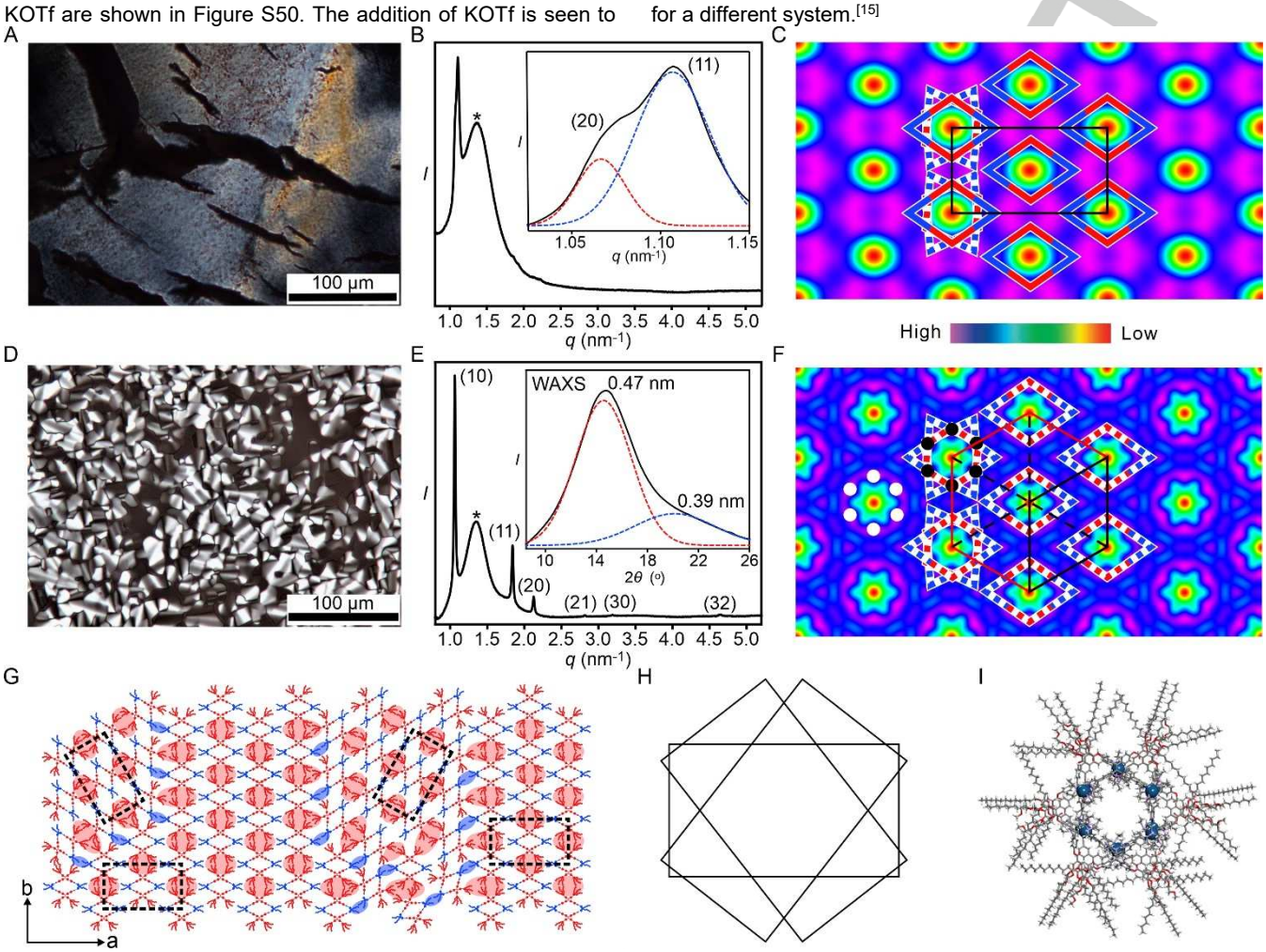

Figure4. Rhomboid **1:** Optical texture of (A) thermotropic and (D) lyotropic LC phase in DMF (18.0 mmol); SAXS diffractogram of (B) thermotropic and(E) lyotropic LC phase in DMF (18.0 mmol); The accompanying WAXS diffractogram is shown in the inset in E; red and blue dotted lines are the resolved peak components; full indaxations of the Col_{rec}/*c2mm* diffractogram is shown in Figure SXX. Reconstructed electron density map of (C) the Col_{rec}/*c2mm* phase (phase combination $\pi\pi\pi\pi\pi\pi$, and (F) Col_{hex}/*p*6mm phase ($\pi\pi\pi\pi0\pi$), with schematic molecules overlaid (blue thick lines denote diplatinum(II) acceptors **9**, red thick lines the ligand **5**); black parallelograms are the crystallographic unit cells. Three equivallent orientations of schematic molecules (dotted lines) after in-plane rotation by -130°, 0°, and +120° are superimposed to give the Star of David patterns giving the global hexagonal symmetry (F); each rhombus has occupancy 1/3; white and black dots indicate the positions of Pt atoms, see also Figure S51. When one direction (molecules with solid lines) becomes preferred, the symmetry breaks and Col_{rec}/*c2mm* phase is formed (C); (G) Schematic representation of an instantaneous arrangement of molecules in the Col_{hex}/*p*6mm phase, containing fluctuating clusters of local rectangular symmetry; but of space-time averaged hexagonal symmetry; the rectangles are local „c2mm" cells, with the red and blue patches representing the local domains of alkyl and tri(ethylene glycol) chains, respectively. (H) Superposition of three local rectangular unit cells obtained by space averaging of the situation in G. (I) Top view of three superimposed rotated molecules; only Pt atoms are shown in CPK mode. The positions of Pt atoms is also shaown as circles in F.

Our interpretation of the X-ray data is that in both the lyotropic hexagonal, and in the thermotropic rectangular phase, the local structure is predominantly rectangular, of the *c2mm* type. That is, within the domain the rhombi are locally parallel to each other. In the hexagonal phase the small domains of local rectangular symmetry are randomly oriented in-plane along the three equivalent 0°, +120° and -120°C axes, with equal probability. The centres of the rhombi have a preferred position on the global hexagonal lattice, giving rise to the sharp Bragg reflections, but their significant deviation from the hexagonal lattice points results in a high Debye-Waller factor greatly suppressing higher diffraction order intensities. Unlike the centres of the molecules, the pendant chains do not lock into the global hexagonal lattice but instead aggregate in clusters with only short-range order – see pink and blue shaded patches in Figure 4G. From the line

width of the resulting diffuse SAXS peak we obtain the average size of local domain as ~31 nm, about 3 unit cell lengths.

The rectangular *c2mm* phase is only a slight distortion of the hexagonal phase, still with local domains along all three directions but now with one of them preferred. The domain size does not increase drastically, since the width of the diffuse peak remains almost unchanged (Figure S49A). In terms of ordering of local centered rectangular clusters, the relationship between the two phases with rectangular and hexagonal long-range order is similar to that between the orthorhombic and hexagonal rotator phases in *n*-alkanes (G Ungar and N Masic, "Order in the rotator phase of n-alkanes", J. Phys. Chem. 1985 89 1036-42.) and in a number of other cases.

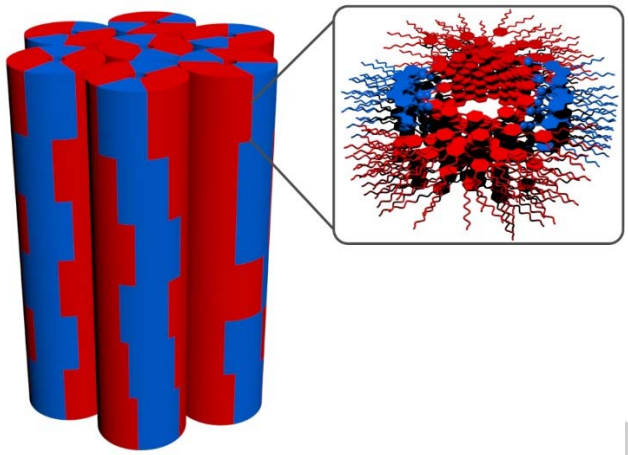

Figure 5. Schematic illustration of the aligned Col_{hex}/*p6*mm structure of lyotropic LC. The blue and red portions stand for local domains of diplatinum(II) acceptors and dipyridyl TPE derivatives, respectively.

Interestingly, the Col_{rec}/*c2mm* – Col_{hex}/*p6mm* transition occurs by the addition of the polar solvent. Accordingly, it is expected that even in the hexagonal phase local domains of rectangular order exist, with three equally probable orientations in the *x*-*y* plane. Actually, in the rectangular phase, the *a*/*b* ratio is about 1.82, which is not too far from the √3 value for a hexagonal phase. The idea is illustrated in Figures 4F and S51 where three local rectangular cells are superimposed to give *global* hexagonal symmetry. Thus, according to this model, even in the Col_{hex}/*p*6mm phase each column is actually non-circular, the XRD gives the time-space average. The reason for the non-circular shape is thought to be the rhombic shape of rhomboid **1**.

Conclusion

In summary, we have designed and synthesized two rhomboidal metallacycles *via* metal-coordination self-assembly. These metallacycles show emission properties both in solution and in the solid state because of the incorporation of TPE derivatives which are typical AIE fluorophores in their structures. More importantly, although neither of the building blocks exhibit mesophases, metallacycles show clear thermotropic and lyotropic liquid crystalline phases, as confirmed by POM, SAXS and WAXS. The formation of metallacylic structures offers a rigid core beneficial for molecular stacking, while the branched alkyl and ethylene glycol chains help stabilize the columnar mesophases. This work provides a simple yet efficient approach to the construction of luminescent metallacycle-cored liquid crystals and explores the use of metal-coordination interactions to induce liquid crystal formation. The materials are of relevance for applications in flat panel displays.

Acknowledgements

This work is supported by the National Natural Science Foundation of China (21801203 to M.Z. and 21761132033, 21374086 to F.L.) and The Key Research and Development Program of Shaanxi Province (2019KW-019 to M.Z.). We thank 111 Project 2.0 (BP2018008) for the financial support and Beamline BL16B1 at SSRF (Shanghai Synchrotron Radiation Facility, China) for providing the beamtimes. We also thank Dr. Gang Chang and Yu Wang at Instrument Analysis Center and Dr. Aqun Zheng at Experimental Chemistry Center of Xi'an Jiaotong University for measurements and Dr. Yu Shao at Peking University for the assistance with part of the SAXS experiments.

Keywords: supramolecular chemistry • aggregation induced emission • metal-coordination • self-assembly • liquid crystals

[1] a) M. O'Neill, S. M. Kelly, *Adv. Mater.* **2003**, *15*, 1135-1146; b) R. Gimenez, M. Pinol, J. L. Serrano, *Chem. Mater.* **2004**, *16*, 1377-1383; c) A. Hayer, V. de Halleux, A. Kohler, A. El-Garoughy, E. W. Meijer, J. Barbera, J. Tant, J. Levin, M. Lehmann, J. Gierschner, J. Cornil, Y. H. Geerts, *J. Phys. Chem. B* **2006**, *110*, 7653-7659; d) Y. Sagara, T. Kato, *Angew. Chem.* **2008**, *120*, 5253-5256; *Angew. Chem. Int. Ed.* **2008**, *47*, 5175-5178; e) R. Cristiano, J. Eccher, I. H. Bechtold, C. N. Tironi, A. A. Vieira, F. Molin, H. Gallardo, *Langmuir* **2012**, *28*, 11590-11598; f) E. Beltran, J. Luis Serrano, T. Sierra, R. Gimenez, *J. Mater. Chem.* **2012**, *22*, 7797-7805; g) C. Tschierske, *Angew. Chem.* **2013**, *125*, 8992-9047; *Angew. Chem. Int. Ed.* **2013**, *52*, 8828-8878; h) Y. F. Wang, J. W. Shi, J. H. Chen, W. G. Zhu, E. Baranoff, *J. Mater. Chem. C.* **2015**, *3*, 7993-8005; i) R. K. Gupta, S. K. Pathak, J. De, S. K. Pal, A. S. Achalkumar, *J. Mater. Chem. C.* **2018**, *6*, 1844-1852.

[2] a) A. C. Sentman, D. L. Gin, *Adv. Mater.* **2001**, *13*, 1398-1401; b) V. de Halleux, J. P. Calbert, P. Brocorens, J. Cornil, J. P. Declercq, J. L. Bredas, Y. Geerts, *Adv. Funct. Mater.* **2004**, *14*, 649-659.

[3] a) J. D. Luo, Z. L. Xie, J. W. Y. Lam, L. Cheng, H. Y. Chen, C. F. Qiu, H. S. Kwok, X. W. Zhan, Y. Q. Liu, D. B. Zhu, B. Z. Tang, *Chem. Commun.* **2001**, 1740-1741; b) Y. N. Hong, J. W. Y. Lam, B. Z. Tang, *Chem. Soc. Rev.* **2011**, *40*, 5361-5388; c) J. Mei, N. L. C. Leung, R. T. K. Kwok, J. W. Y. Lam, B. Z. Tang, *Chem. Rev.* **2015**, *115*, 11718-11940; d) Z. J. Zhao, J. W. Y. Lam, B. Z. Tang, *J. Mater. Chem.* **2012**, *22*, 23726-23740; e) J. Mei, Y. N. Hong, J. W. Y. Lam, A. J. Qin, Y. H. Tang, B. Z. Tang, *Adv. Mater.* **2014**, *26*, 5429-5479; f) J. Huang, H. Nie, J. Zeng, Z. Zhuang, S. Gan, Y. Cai, J. Guo, S. J. Su, Z. Zhao, B. Z. Tang, *Angew. Chem.* **2017**, *129*, 13151-13156; *Angew. Chem. Int. Ed.* **2017**, *56*, 12971-12976; g) H. Liu, J. Zeng, J. Guo, H. Nie, Z. Zhao, B. Z. Tang, *Angew. Chem.* **2018**, *130*, 9434-9438; *Angew. Chem. Int. Ed.* **2018**, *57*, 9290-9294.

[4] a) W. Z. Yuan, Z. Q. Yu, P. Lu, C. M. Deng, J. W. Y. Lam, Z. M. Wang, E. Q. Chen, Y. G. Ma, B. Z. Tang, *J. Mater. Chem.* **2012**, *22*, 3323-3326; b) J. Kim, S. Cho, B. K. Cho, *Chem. Eur. J.* **2014**, *20*, 12734-12739; c) X. Yu, H. Chen, X. Shi, P.-A. Albouy, J. Guo, J. Hu, M.-H. Li, *Mater. Chem. Front.* **2018**, *2*, 2245-2253; d) D. Y. Zhao, F. Fan, J. Cheng, Y. L. Zhang, K. S. Wong, V. G. Chigrinov, H. S. Kwok, L. Guo, B. Z. Tang, *Adv. Opt. Mater.* **2015**, *3*, 199-202; e) D. Y. Zhao, F. Fan, V. G. Chigrinov, H. S. Kwok, B. Z. Tang, *J. Soc. Inf. Disp.* **2015**, *23*, 218-222.

[5] For reviews, see: a) S. Leininger, B. Olenyuk, P. J. Stang, *Chem. Rev.* **2000**, *100*, 853-907; b) M. Fujita, M. Tominaga, A. Hori, B. Therrien, *Acc. Chem. Res.* **2005**, *38*, 369-378; c) C. G. Oliveri, P. A. Ulmann, M. J.

Wiester, C. A. Mirkin, *Acc. Chem. Res.* **2008**, *41*, 1618-1629; d) B. H. Northrop, Z. Yao-Rong, C. Ki-Whan, P. J. Stang, *Acc. Chem. Res.* **2010**, *41*, 1554-1563; e) T. R. Cook, Y.-R. Zheng, P. J. Stang, *Chem. Rev.* **2013**, *113*, 734-777; f) T. R. Cook, P. J. Stang, *Chem. Rev.* **2015**, *115*, 7001-7045; g) G. R. Newkome, C. N. Moorefield, *Chem. Soc. Rev.* **2015**, *44*, 3954-3967; h) A. J. Mcconnell, C. S. Wood, P. P. Neelakandan, J. R. Nitschke, *Chem. Rev.* **2015**, *115*, 7729-7793; i) L. J. Chen, H. B. Yang, M. Shionoya, *Chem. Soc. Rev.* **2017**, *46*, 2555-2576; j) J. Uchida, M. Yoshio, S. Sato, H. Yokoyama, M. Fujita, T. Kato, *Angew. Chem.* **2017**, *129*, 14273-14277; *Angew. Chem. Int. Ed.* **2017**, *56*, 14085-14089; k) L. J. Chen, H. B. Yang, *Acc. Chem. Res.* **2018**; *51*, 2699-2710; l) H. Sepehrpour, W. X. Fu, Y. Sun, P. J. Stang, *J. Am. Chem. Soc.* **2019**, *141*, 14005-14020.

[6] For some research articles on SCCs, see: a) M. Wang, Y.-R. Zheng, K. Ghosh, P. J. Stang, *J. Am. Chem. Soc.* **2010**, *132*, 6282-6283; b) N. Kishi, Z. Li, K. Yoza, M. Akita, M. Yoshizawa, *J. Am. Chem. Soc.* **2011**, *133*, 11438-11441; (c) K. Li, L.-Y. Zhang, C. Yan, S.-C. Wei, M. Pan, L. Zhang, C.-Y. Su, *J. Am. Chem. Soc.* **2014**, *136*, 4456-4459; d) D. Fujita, Y. Ueda, S. Sato, N. Mizuno, T. Kumasaka, M. Fujita, *Nature* **2016**, *540*, 563-566; e) W. Cullen, M. C. Misuraca, C. A. Hunter, N. H. Williams, M. D. Ward, *Nat. Chem.* **2016**, *8*, 231-236; f) L. Zhang, L. Lin, D. Liu, Y. J. Lin, Z. H. Li, G. X. Jin, *J. Am. Chem. Soc.* **2017**, *139*, 1653-1660; g) B. Song, Z. Zhang, K. Wang, C. H. Hsu, O. Bolarinwa, J. Wang, Y. Li, G. Q. Yin, E. Rivera, H. B. Yang, C. Liu, B. Xu, X. Li, *Angew. Chem.* **2017**, *129*, 5342-5346; *Angew. Chem. Int. Ed.* **2017**, *56*, 5258-5262; h) P. Howlader, B. Mondal, P. C. Purba, E. Zangrando, P. S. Mukherjee, *J. Am. Chem. Soc.* **2018**, *140*, 7952-7960; i) L.-X. Cai, S.-C. Li, D.-N. Yan, L.-P. Zhou, F. Guo, Q.-F. Sun, *J. Am. Chem. Soc.* **2018**, *140*, 4869-4876; j) W. Zheng, W. Wang, S. T. Jiang, G. Yang, Z. Li, X. Q. Wang, G. Q. Yin, Y. Zhang, H. Tan, X. Li, H. Ding, G. Chen, H. B. Yang, *J. Am. Chem. Soc.* **2019**, *141*, 583-591; k) L. Zhang, R. Das, C. T. Li, Y. Y. Wang, F. E. Hahn, K. Hua, L. Y. Sun, Y. F. Han, *Angew. Chem.* **2019**, *131*, 13494-13498; *Angew. Chem. Int. Ed.* **2019**, *58*, 13360-13364.

[7] a) X. Yan, T. R. Cook, P. Wang, F. Huang, P. J. Stang, *Nat. Chem.* **2015**, *7*, 342-348; b) X. Yan, H. Wang, C. E. Hauke, T. R. Cook, M. Wang, M. L. Saha, Z. Zhou, M. Zhang, X. Li, F. Huang, P. J. Stang, *J. Am. Chem. Soc.* **2015**, *137*, 15276-15286; c) X. Yan, M. Wang, T. R. Cook, M. Zhang, M. L. Saha, Z. Zhou, X. Li, F. Huang, P. J. Stang, *J. Am. Chem.Soc.* **2016**, *138*, 4580-4588; d) M. L. Saha, X. Yan, P. J. Stang, *Acc. Chem. Res.* **2017**, *49*, 2527-2539; e) C. Lu, M. Zhang, D. Tang, X. Yan, Z. Zhang, Z. Zhou, B. Song, H. Wang, X. Li, S. Yin, H. Sepehrpour, P. J. Stang, *J. Am. Chem. Soc.* **2018**, *140*, 7674-7680.

[8] a) M. Zhang, M. L. Saha, M. Wang, Z. Zhou, B. Song, C. Lu, X. Yan, X. Li, F. Huang, S. Yin, P. J. Stang, *J. Am. Chem. Soc.* **2017**, *139*, 5067-5074; b) Z. Zhang, Z. Zhao, L. Wu, S. Lu, S. Ling, G. Li, L. Xu, L. Ma, Y. Hou, X. Wang, X. Li, G. He, K. Wang, B. Zou, M. Zhang, J. Am. Chem. Soc. **2020**, *142*, 2592-2600.

[9] M. Zhang, S. Yin, J. Zhang, Z. Zhou, M. L. Saha, C. Lu, P. J. Stang, *Proc. Natl. Acad. Sci. USA* **2017**, *114*, 3044-3049.

[10] M. Zhang, S. Li, X. Yan, Z. Zhou, M. L. Saha, Y. Wang, P. J. Stang, *Proc. Natl. Acad. Sci. USA* **2016**, *113*, 11100-11105.

[11] Z. Zhang, Z. Zhao, Y. Hou, H. Wang, X. Li, G. He, M. Zhang, *Angew. Chem.* **2019**, *131*, 8954-8958; *Angew. Chem. Int. Ed.* **2019**, *58*, 8862-8866.

[12] G. Q. Yin, H. Wang, X. Q. Wang, B. Song, L. J. Chen, L. Wang, X. Q. Hao, H. B. Yang, X. Li, *Nat. Commun.* **2018**, *9*, 567.

[13] a) V. N. Kozhevnikov, B. Donnio, D. W. Bruce, *Angew. Chem. Int. Ed.* **2008**, *47*, 6286-6289; b) M. Krikorian, S. Liu, T. M. Swager, *J. Am. Chem. Soc.* **2014**, *136*, 2952-2955; c) X. Wu, G. Xie, C. P. Cabry, X. Xu, S. J. Cowling, D. W. Bruce, W. Zhu, E. Baranoff, Y. Wang, *J. Mater. Chem. C.* **2018**, *6*, 3298-3309.

[14] a) M. Fritzsche, A. Bohle, D. Dudenko, U. Baumeister, D. Sebastiani, G. Richardt, H. W. Spiess, M. R. Hansen, S. Hoger, *Angew. Chem.* **2011**, *123*, 3086-3089; *Angew. Chem. Int. Ed.* **2011**, *50*, 3030-3033; b) S.-i. Kawano, Y. Ishida, K. Tanaka, *J. Am. Chem. Soc.* **2015**, *137*, 2295-2302; c) T. Wohrle, I. Wurzbach, J. Kirres, A. Kostidou, N. Kapernaum, J. Litterscheidt, J. C. Haenle, P. Staffeld, A. Baro, F. Giesselmann, S. Laschat, *Chem. Rev.* **2016**, *116*, 1139-1241; d) S. Wu, Y. Li, S. Xie, C. Ma, J. Lim, J. Zhao, D. S. Kim, M. Yang, D. K. Yoon, M. Lee, S. O. Kim, Z. Huang, *Angew. Chem.* **2017**, *129*, 11669-11672; *Angew. Chem. Int. Ed.* **2017**, *56*, 11511-11514; e) S. I. Kawano, M. Kato, S. Soumiya, M. Nakaya, J. Onoe, K. Tanaka, *Angew. Chem.* **2018**, *130*, 8954-8958; *Angew. Chem. Int. Ed.* **2018**, *57*, 173-177; f) M. Lehmann, M. Dechant, M. Lambov, T. Ghosh, *Acc. Chem. Res.* **2019**, *52*, 1653-1664; g) J. De, I. Bala, S. P. Gupta, U. K. Pandey, S. K. Pal, *J. Am. Chem. Soc.* **2019**, *141*, 18799-18805.

[15] a) J. A. Schröter, C. Tschierske, M. Wittenberg, J. H. Wendorff, *J. Am. Chem. Soc.* **1998**, *120*, 10669-10675; b) A. Lehmann, M. Prehm, C. Chen, F. Liu, X. Zeng, G. Ungar, C. Tschierske, *Chem. Commun.* **2018**, *54*, 12306-12309.

Entry for the Table of Contents

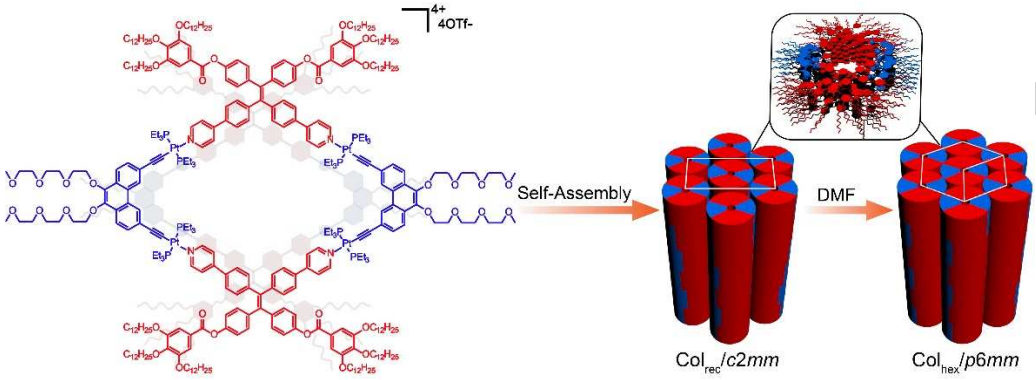

Luminescent Metallacycle-Cored Liquid Crystals

Based on metal-coordination-driven self-assembly, two luminescent rhomboidal metallacycles with aggregation induced emission properties were prepared. One of the metallacycles also exhibited liquid crystals due to the intermolecular packing of the metallacycles, indicating that the liquid crystal properties could be induced by metal-coordination interactions.

Long Chen, Changlong Chen, Yue Sun, Shuai Lu, Haohui Huo, Tianyi Tan, Anquan Li, Xiaopeng Li, Goran Ungar, Feng Liu, and Mingming Zhang**

Luminescent Metallacycle-Cored Liquid Crystals Induced by Metal-Coordination